

Floquet analysis of real-time wave functions without solving the Floquet equation

V. Kapoor and D. Bauer

Institut für Physik, Universität Rostock, D-18051 Rostock, Germany

(Received 7 October 2011; published 16 February 2012)

We propose a method to obtain Floquet states—also known as light-induced states—and their quasienergies from real-time wave functions without solving the Floquet equation. This is useful for the analysis of various phenomena in time-dependent quantum dynamics if the Hamiltonian is not strictly periodic, as in short laser pulses, for instance. There, the population of the Floquet states depends on the pulse form and is automatically contained in the real-time wave function but not in the standard Floquet approach. Several examples in the area of intense laser-atom interaction are exemplarily discussed: (i) the observation of even harmonics for an inversion-symmetric potential with a single bound state; (ii) the dependence of the population of Floquet states on (gauge) transformations and the emergence of an invariant, observable photoelectron spectrum; (iii) the driving of resonant transitions between dressed states, (i.e., the dressing of dressed states), and (iv) spectral enhancements at channel closings due to the ponderomotive shift of above-threshold ionization peaks.

DOI: [10.1103/PhysRevA.85.023407](https://doi.org/10.1103/PhysRevA.85.023407)

PACS number(s): 32.80.Rm, 02.70.Hm, 32.80.Wr

I. INTRODUCTION

The time-dependent Schrödinger equation (TDSE) with a time-periodic Hamiltonian has solutions which can be expressed in a time-periodic basis. This basis is referred to as the Floquet basis, and eigenstates in this basis are the Floquet states [1–4]. Time-periodic potentials naturally arise when matter is exposed to laser fields. In this context, Floquet states are also known as “light-induced states” (LISs) [5], because they are the new states of the combined system “target + laser field.” In fact, Floquet theory has been used to determine, for example, very accurate ionization rates [6,7]. Using so-called R -matrix Floquet theory, the method has been extended to multielectron systems [8]. Strict periodicity of the Hamiltonian with the laser period implies physically that the laser pulse was always on and will be on forever. Then the problem arises of how the field-free system under study (e.g., an atom) gets into the laser field in the first place and how the field-free observables emerge. In fact, the population of the Floquet states depends on the laser pulse form. If the (up and down) ramping of the laser field is adiabatic and the laser frequency is nonresonant we expect the system to follow just a single Floquet state; namely, the one which is adiabatically connected to the field-free initial state. However, for nonadiabatic ramping or resonant interactions, a superposition of Floquet states is created. An example for nonadiabatic population of several Floquet states, leading to an apparent generation of even harmonics in inversion-symmetric potentials, is given in Sec. III of this paper.

Instead of converting the TDSE into the time-independent Floquet equation [Eq. (13) below] one may alternatively solve it directly in real time. In the latter case there are no assumptions about periodicity or adiabatic ramping and, for example, the effect of different laser pulse forms can be studied. However, the direct solution of the TDSE in real time does not involve the Floquet basis, so that information about LISs is not directly available. As many interesting phenomena such as the ac Stark effect, Rabi oscillations, or stabilization against ionization [9,10] are most conveniently analyzed in terms of LISs, it is desirable to extract the “Floquet information” from the real-time wave function “on the fly”

while propagating (or by postprocessing) it, without having to solve the Floquet equation as well. We present such a method to analyze nonperturbative, laser-driven quantum dynamics via the (time-resolved) Floquet information contained in the corresponding real-time wave function.

The paper is organized as follows: in Sec. II we review the basics of Floquet theory. In Sec. III we briefly summarize the general derivation of harmonic generation selection rules before we present the (at first sight surprising) presence of peaks at even harmonics of the laser frequency in the case of an inversion-symmetric potential with only one bound state. In Sec. IV we introduce our method to obtain the Floquet information from the real-time wave function (e.g., the populated states and their energies) and use them to explain the presence of hyper-Raman lines at even harmonic frequencies. In Sec. V we investigate how the population of Floquet states changes under (gauge) transformations while the Floquet energies and the observable photoelectron spectra remain invariant. In Sec. VI time-resolved Floquet spectra of real-time wave functions in the so-called velocity gauge and in the Kramers-Henneberger frame of reference are compared. In Sec. VII the channel-closing phenomenon and related spectral enhancements are interpreted in terms of Floquet state-crossings. A conclusion is given in Sec. VIII. In this work we restrict ourselves to spatially one-dimensional (1D) model Hamiltonians. It is straightforward to extend the method to higher dimensions, as indicated in Appendix. Atomic units (a.u.) $|e| = m_e = \hbar = 4\pi\epsilon_0 = 1$ are used unless noted otherwise.

II. BASIC THEORY

Consider a linearly polarized laser field $E(t)$ of frequency ω_1 in the dipole approximation, polarized along the x direction and interacting with an electron in some binding potential V . The Hamiltonian in length gauge reads

$$\hat{H}(t) = \hat{H}_0 + \hat{W}(x,t), \quad \hat{W}(x,t) = xE(t), \quad (1)$$

with

$$\hat{H}_0 = -\frac{1}{2} \frac{\partial^2}{\partial x^2} + V(x). \quad (2)$$

A. Floquet theory

For sufficiently long laser pulses

$$E(t+T) = E(t), \quad T = \frac{2\pi}{\omega_1}, \quad (3)$$

holds to high accuracy, and thus also $\hat{W}(t+T) = \hat{W}(t)$, so that

$$\hat{H}(t+T) = \hat{H}(t). \quad (4)$$

The Floquet theorem [1–4] states that, in this case, the TDSE

$$i \frac{\partial}{\partial t} \Psi(x,t) = \hat{H}(t) \Psi(x,t) \quad (5)$$

has solutions of the form

$$\Psi(x,t) = e^{-i\epsilon t} \Phi(x,t), \quad (6)$$

$\Phi(x,t)$ being periodic itself,

$$\Phi(x,t) = \Phi(x,t+T). \quad (7)$$

The quantity ϵ is called the quasienergy or Floquet energy. The wave functions $\Phi(x,t)$ fulfill the Schrödinger equation

$$\hat{\mathcal{H}}(t) \Phi(x,t) = \epsilon \Phi(x,t), \quad (8)$$

with

$$\hat{\mathcal{H}}(t) = \hat{H}(t) - i \frac{\partial}{\partial t}. \quad (9)$$

If ϵ is an eigenvalue and $\Phi(x,t)$ the corresponding eigenstate, also

$$\epsilon' = \epsilon + m\omega_1, \quad \Phi'(x,t) = e^{im\omega_1 t} \Phi(x,t), \quad m \in \mathbb{Z} \quad (10)$$

are solutions of (8). Owing to the time periodicity of $\Phi(x,t)$, we can expand

$$\Phi(x,t) = \sum_{n=-\infty}^{\infty} \varphi_n(x) e^{-in\omega_1 t}. \quad (11)$$

For a monochromatic laser field the interaction Hamiltonian $\hat{W}(x,t)$ can be written as

$$\hat{W}(x,t) = \hat{W}^+(x) \exp(i\omega_1 t) + \hat{W}^-(x) \exp(-i\omega_1 t), \quad (12)$$

leading to the time-independent Floquet equation

$$(\epsilon + n\hbar\omega_1 - \hat{H}_0) \varphi_n(x) = \hat{W}^+(x) \varphi_{n+1}(x) + \hat{W}^-(x) \varphi_{n-1}(x). \quad (13)$$

The index n of the Floquet state is known as the ‘‘block index,’’ which may be interpreted as the number of photons involved in the process under study. Hence, the Floquet equation (13) couples any Floquet block n with its neighboring blocks $n \pm 1$ via absorption or emission of a photon.

In principle, (13) is an infinite-dimensional set of differential equations. In practice, it is truncated so that $n_{\min} \leq n \leq n_{\max}$. In obtaining the eigenvalue equation (13), we assumed strict time periodicity, which physically means that the laser pulse is always on.

B. Non-Hermitian Floquet Theory

We are interested in systems which, in the field-free situation, possess besides bound states also a continuum. In the presence of a laser field, such a system may ionize; that is, the field-free stationary states are turned into field-dressed, quasistationary states. The simplest cases of only a few (field-free) bound states (allowing for resonances) plus a continuum dressed by laser fields have been discussed in the literature since long ago (see, e.g., [11] and [12] for a review). In an actual implementation of Floquet theory, the decay of quasistationary states needs to be taken into account when solving (13) by applying Siegert boundary conditions for the outgoing waves [7], leading to complex Floquet energies

$$\epsilon = \text{Re}\epsilon - i \frac{\Gamma}{2}, \quad (14)$$

where Γ is the ionization rate. The difference between $\text{Re}\epsilon$ and the field-free $\epsilon^{(0)}$ is the ac Stark shift.

C. Finite-grid, finite-pulse TDSE solution

We solve

$$i \frac{\partial}{\partial t} \Psi_{\#}(x,t) = \hat{H}(t) \Psi_{\#}(x,t) \quad (15)$$

on a numerical grid of size L ($-\frac{L}{2} < x < \frac{L}{2}$) for times $0 < t < t_{\text{sim}}$ with t_{sim} being the total simulation time. The binding potential $V(x)$ is centered at $x = 0$. In all cases discussed in this work we start from the field-free ground state on the grid $\Psi_{\#}(x,0) = \Psi_{\#}^{(0)}(x)$. The probability density approaching the grid boundary is absorbed by an imaginary potential.

Our aim in the following will be to analyze $\Psi_{\#}(x,t)$ in terms of Floquet energies and states.

III. HARMONIC GENERATION

In the first example we apply our method to investigate the origin of apparently even harmonics in an inversion-symmetric potential with only one bound state.

There are many ways to derive selection rules for harmonic generation (HG). Most elegant, rigorous, and appropriate for our purpose is the approach employing dynamical symmetries [13,14]. Consider the stationary Schrödinger equation

$$\hat{H}_0 \Psi(x) = \mathcal{E} \Psi(x), \quad (16)$$

with \hat{H}_0 given by (2). If the potential V is inversion-symmetric, $V(x) = V(-x)$, the Hamiltonian \hat{H}_0 is invariant under spatial inversion as well,

$$\hat{P}_p f(x) = f(-x), \quad \hat{P}_p^2 = 1, \quad \hat{P}_p^{-1} = \hat{P}_p, \quad (17)$$

$$[\hat{H}_0, \hat{P}_p] = 0, \quad (18)$$

so that, for nondegenerate energies \mathcal{E} , the eigenstate $\Psi(x)$ is also an eigenstate of the spatial-inversion operator \hat{P}_p . Because of $\hat{P}_p^2 = 1$ the eigenvalues can only be ± 1 (parity):

$$\hat{P}_p \Psi(x) = \pm \Psi(x). \quad (19)$$

The full Hamiltonian (1) and the Floquet-Hamiltonian (9) are not invariant under spatial inversion but under the

dynamical symmetry operation “spatial inversion combined with a translation in time by half a period,”

$$[\hat{H}(t), \hat{P}_{pt}] = [\hat{\mathcal{H}}(t), \hat{P}_{pt}] = 0, \quad (20)$$

$$\hat{P}_{pt} f(x, t) = f(-x, t + \pi/\omega_1), \quad \hat{P}_{pt}^2 = 1, \quad (21)$$

$$\hat{P}_{pt} = \hat{P}_p \hat{P}_t = \hat{P}_t \hat{P}_p, \quad \hat{P}_t f(x, t) = f(x, t + \pi/\omega_1). \quad (22)$$

For nondegenerate ϵ ,

$$\hat{P}_{pt} \Phi(x, t) = \pm \Phi(x, t). \quad (23)$$

Because of (11) we observe that

$$\hat{P}_{pt} \Phi(x, t) = \sum_n (-1)^n e^{-in\omega_1 t} \hat{P}_p \varphi_n(x), \quad (24)$$

and, with (23), it follows that

$$\hat{P}_p \varphi_n(x) = \pm (-1)^n \varphi_n(x); \quad (25)$$

that is, the $\varphi_n(x)$ have an alternating parity with respect to the Floquet block index n .

Numerically, the HG spectrum $\sim \omega^4 |d(\omega)|^2$ is calculated via the Fourier-transformed dipole moment

$$d(\omega) \sim \int_0^{t_{\text{sim}}} dt \int_{-\frac{L}{2}}^{\frac{L}{2}} dx \Psi_{\#}^*(x, t) x \Psi_{\#}(x, t) e^{i\omega t}. \quad (26)$$

Assuming that the numerically determined exact wave function on the grid is well described by just a single Floquet state, using (6), (11), and (14) yields

$$d(\omega) \sim \sum_{nm} \int_{-\frac{L}{2}}^{\frac{L}{2}} \varphi_m^*(x) x \varphi_n(x) dx \times \int_0^{t_{\text{sim}}} e^{t\{i[\omega - \omega_1(n-m)] - \Gamma\}} dt. \quad (27)$$

The spatial integral is nonvanishing only if φ_n has the opposite parity of φ_m ; namely,

$$n - m = 2k + 1, \quad k \in \mathbb{Z}. \quad (28)$$

The temporal integral thus leads to peaks centered at frequencies

$$\omega = (2k + 1)\omega_1, \quad (29)$$

with widths determined by t_{sim} (frequency-time uncertainty) and Γ (decay). The selection rule (29) is the well-known result that an inversion-symmetric target in a linearly polarized laser field generates *odd* harmonics only. Note that the above derivation also holds for multielectron targets because the electron-electron interaction is also invariant under the symmetry operations \hat{P}_p and \hat{P}_{pt} .

A. Hyper-Raman lines at even harmonics of laser frequency

It is known that HG peaks at positions different from odd multiples of the fundamental laser frequency ω_1 are to be expected for an inversion-symmetric potential if at least two Floquet states of opposite parity are populated [15,16]. Physically, the superposition of two Floquet states may amount to, for example, the absorption of n photons of energy ω_1 but emission of one photon of energy $n\omega_1 - \Delta\epsilon$, with $\Delta\epsilon$ being the energy difference between initial and final states. This should

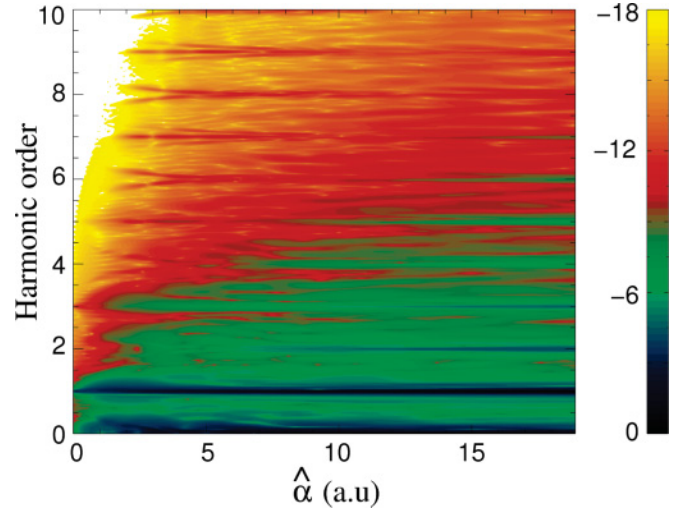


FIG. 1. (Color online) Logarithmically scaled HG strength $\omega^4 |d(\omega)|^2$ vs harmonic order and excursion amplitude $\hat{\alpha} = \hat{A}/\omega_1$ [$\omega_1 = 1$, vector potential $A(t)$ ramped up and down over 4 cycles and held constant with amplitude \hat{A} for 30 cycles]. The numerical fast-Fourier transform was performed over the pulse duration (i.e., $t_{\text{sim}} = 38$ cycles), using a Hanning window.

lead to hyper-Raman lines in the spectra which, however, are typically weak [16,17]. Nevertheless, if observable, they appear at even harmonics of the laser frequency in the case of degeneracy, $\Delta\epsilon = 0$.

We consider an electron in the Pöschl-Teller potential

$$V(x) = -\frac{1}{\cosh^2 x} \quad (30)$$

and subject to a laser field. The potential (30) supports only a single bound state $\Psi_0(x)$ of energy $\mathcal{E}_0 = -0.5$. Hence, superpositions of field-free bound states are ruled-out. As a consequence, perturbation theory in the external field can certainly not predict hyper-Raman lines or even harmonics. However, Fig. 1 shows the logarithmically scaled HG strength $\omega^4 |d(\omega)|^2$ as obtained from the numerical solution of the TDSE. The HG strength is plotted vs harmonic order ω/ω_1 and the amplitude $\hat{\alpha}$ of the excursion

$$\alpha(t) = \int^t A(t) dt, \quad (31)$$

with $A(t)$ being the vector potential of the laser field. The electric field is given by $E(t) = -\partial_t A(t)$. Given the vector potential amplitude \hat{A} , the excursion amplitude is $\hat{\alpha} = \hat{A}/\omega_1$, the field amplitude $\hat{E} = \hat{A}\omega_1$. The laser pulse parameters are specified in the figure caption. One sees that, for sufficiently strong excursion amplitude $\hat{\alpha}$, peaks at even harmonics of the laser frequency appear, too. Picking an even harmonic at $\hat{\alpha} > 15$ (e.g., the 6th) and tracing it back to low $\hat{\alpha}$ reveals that the peak splits and rapidly drops in magnitude (e.g., around $\hat{\alpha} \simeq 2$ for the 6th harmonic). In the next section we will use our real-time Floquet method to show that the appearance of even harmonics is due to the population of several LISs that become quasidegenerate as $\hat{\alpha}$ increases.

B. Superposition of Floquet states

In the case of a nonadiabatic transfer of the field-free state to field-dressed states one has to allow for a superposition of Floquet states in order to represent the exact, numerically determined wave function on the grid,

$$\Psi_{\#}(x,t) \simeq \sum_{\beta} e^{-i\epsilon_{\beta}t} \Phi_{\beta}(x,t) = \sum_{\beta n} e^{-it(\epsilon_{\beta}+n\omega_1)} \varphi_{\beta n}(x). \quad (32)$$

Here we assume that the expansion coefficients are included in $\Phi_{\beta}(x,t)$ and $\varphi_{\beta n}(x)$. For continuous quasienergies, the sum over β should be replaced by an integral over ϵ . The Fourier-transformed dipole will be

$$d(\omega) \sim \sum_{\beta\gamma nm} \int_{-\frac{1}{2}}^{\frac{1}{2}} \varphi_{\gamma m}^*(x) x \varphi_{\beta n}(x) dx \times \int_0^{t_{\text{sim}}} e^{it\{i[\omega-\omega_1(n-m)-(\text{Re}\epsilon_{\beta}-\text{Re}\epsilon_{\gamma})]-(\Gamma_{\beta}+\Gamma_{\gamma})/2\}} dt. \quad (33)$$

Again, in order for the spatial integral to not vanish, the parity of $\varphi_{\beta n}$ and $\varphi_{\gamma m}$ must be different. However, now this can be the case not only for $n-m=2k+1$, but also for $n-m=2k$ if the parity of, for example, $\varphi_{\beta 0}$ is opposite to that of $\varphi_{\gamma 0}$. Hence, one expects the above-mentioned hyper-Raman peaks at

$$\omega = k\omega_1 + \Delta\epsilon, \quad k \in \mathbb{Z}, \quad (34)$$

where $\Delta\epsilon = \text{Re}\epsilon_{\beta} - \text{Re}\epsilon_{\gamma}$ is the difference between the real parts of the two Floquet quasienergies involved. Thus, in order to observe even harmonics at exactly $\omega = 2k\omega_1$ a degeneracy $\text{Re}\epsilon_{\beta} = \text{Re}\epsilon_{\gamma}$ is required. Such a degeneracy between the (field-dressed) initial state and another one of opposite parity is also likely to populate the latter one.

IV. FLOQUET-STATE ANALYSIS OF REAL-TIME WAVE FUNCTIONS

The extraction of Floquet information contained in the real-time wave function is useful to analyze any feature of interest in HG spectra. We start with the determination of the (real part of the) quasienergy of the populated Floquet states. Once these energies are known, the corresponding Floquet states can be obtained. The method is similar to the one proposed in [18] for field-free dynamics.

The numerical solution of the time-dependent Schrödinger equation in real time yields $\Psi_{\#}(x,t)$. Upon multiplication of (32) by an even or odd test function $q_{\pm}(x)$, spatial integration, and Fourier transformation from the time to the energy domain,

$$Q_{\pm}(\mathcal{E}) = \sum_{\beta n} \int_{t_1}^{t_2} e^{-it(\epsilon_{\beta}+n\omega_1-\mathcal{E})} dt \int_{-\frac{1}{2}}^{\frac{1}{2}} q_{\pm}(x) \varphi_{\beta n}(x) dx, \quad (35)$$

with $0 \leq t_1 < t_2 \leq t_{\text{sim}}$, one can extract from the peak positions in $|Q_{\pm}(\mathcal{E})|^2$ the real part of the Floquet energies

$$\text{Re}\mathcal{E}_{\beta n} = \text{Re}\epsilon_{\beta} + n\omega_1 \quad (36)$$

belonging to even or odd Floquet states $\varphi_{\beta n}$, respectively. The even test function is, for example, simply unity for all $-\frac{1}{2} < x < \frac{1}{2}$, the odd test function may be chosen to be 1 for $x > 0$

and -1 for $x < 0$. The purpose of these test functions is to extract the even- and odd-parity Floquet states separately. Of course, only the energies of the populated (and thus relevant) Floquet states $\varphi_{\beta n}$ are obtained in this way.

The imaginary part $\Gamma_{\beta}/2$ of ϵ_{β} contributes to the width of the peaks in $|Q_{\pm}(\mathcal{E})|^2$. However, in our finite-time, finite-grid TDSE simulations the width of the peaks in $|Q_{\pm}(\mathcal{E})|^2$ also depend on the integration time $t_2 - t_1$ and the grid-size because of the absorbing grid boundaries. Only for a flat-top laser pulse and a very long simulation time would a stationary absorption rate at the grid boundaries be established, and Γ_{β} could be determined from the peak width. This, however, is exactly the regime where the standard Floquet approach should be applied. We focus here on aspects of our method complementary to the conventional Floquet method, in particular its applicability to finite pulses and time-resolved studies.

If we multiply the wave function (32) by $\exp(it\mathcal{E})$ (with \mathcal{E} real) and integrate over time, mainly the Floquet state $\varphi_{\mathcal{E}}$ for which the phase is stationary (i.e., $\mathcal{E} = \text{Re}\epsilon_{\beta} + n\omega_1$) “survives,”

$$\varphi_{\mathcal{E}}(x) \sim \int_{t_1}^{t_2} e^{it\mathcal{E}} \Psi_{\#}(x,t) dt. \quad (37)$$

The integration time $t_2 - t_1$ has to be sufficiently long in order to cover many temporal oscillations of the wave function.

Starting from the ground state in the potential (30), we solved the TDSE for a high-frequency laser field of vector potential $A(t) = -\hat{A}(t) \sin \omega_1 t$ for $\omega_1 = 4$ and $\hat{A}(t)$ a trapezoidal pulse shape with linear up and down ramps over 4 cycles and 1200 cycles constant amplitude \hat{A} [denoted in the form (4, 1200, 4) in the following]. Figure 2 shows

$$R = |Q_+|^2 + |Q_-|^2 \quad (38)$$

[with the time-integral in (35) performed over the entire pulse] as a contour plot vs the excursion amplitude $\hat{\alpha} = \hat{A}/\omega_1$ and energy \mathcal{E} for an energy interval within the zeroth Floquet block

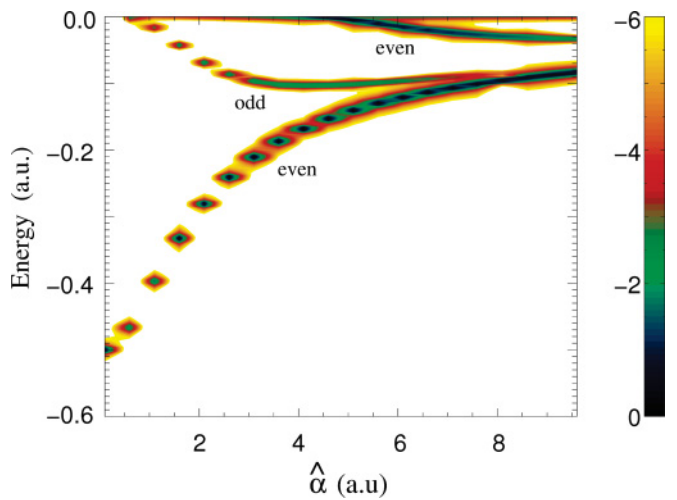


FIG. 2. (Color online) Logarithmic plot of $R = |Q_+|^2 + |Q_-|^2$ vs energy \mathcal{E} and excursion amplitude $\hat{\alpha} = \hat{A}/\omega_1$, showing the quasienergies of the (populated) field-dressed states. The laser frequency was $\omega_1 = 4$. The pulse shape was trapezoidal (4, 1200, 4) in the vector potential of amplitude \hat{A} . For each $\hat{\alpha}$ the maximum in R was renormalized to unity.

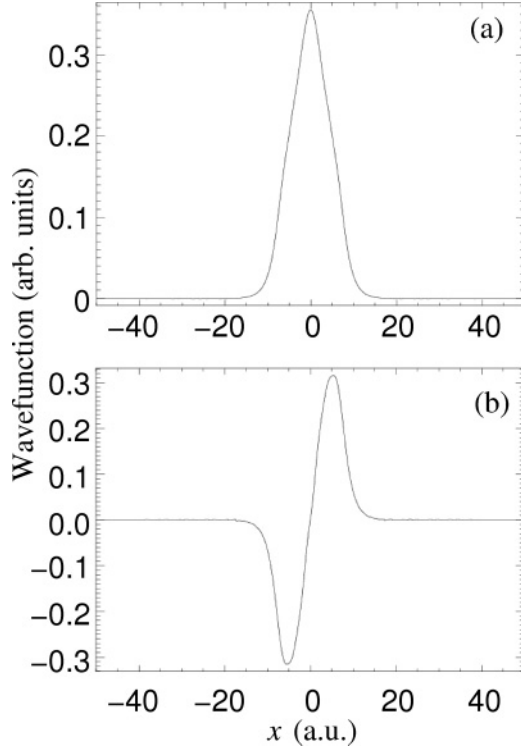


FIG. 3. Field-dressed ground-state wave function $\tilde{\varphi}_{0n}$ for $\hat{\alpha} = 4$. (a) Floquet block $n = 0$, (b) $n = -1$.

$n = 0$. Plotting $|Q_+|^2$ and $|Q_-|^2$ individually allows us to distinguish the parity of the states (labeled “even” or “odd” in Fig. 2). For $\hat{\alpha} \rightarrow 0$ only the field-free state at $\mathcal{E} = -0.5$ remains. However, with increasing excursion amplitude $\hat{\alpha}$, light-induced quasibound states emerge, which are populated due to the finite rise time of the laser field. From the populations (see color coding) one infers that, around $\hat{\alpha} = 6$, besides the field-dressed ground state the second-excited field-dressed state is more populated than the first excited. For increasing $\hat{\alpha}$, the field-dressed ground state and the field-dressed first-excited state become almost degenerate so that $\Delta\epsilon \rightarrow 0$ in (34), explaining the peaks at even harmonics of the laser frequency due to hyper-Raman scattering.

Using (37) we extracted field-dressed states. Figure 3 shows the field-dressed ground state for the Floquet blocks $n = 0$ (a) and $n = -1$ (b) for $\hat{\alpha} = 4$. The integration time was again the pulse duration. Equation (37) in general yields a complex wave function $\varphi_{\mathcal{E}} = \tilde{\varphi}_{\mathcal{E}} e^{i\theta}$. The plots in Fig. 3 show the real wave function $\tilde{\varphi}_{\mathcal{E}}$. It is seen that the parity indeed changes as one decreases n by one. For $n = 0$ and $\hat{\alpha} = 0$ the ground state must be even. Hence, for $n = -1$ it is odd, in accordance with (25).

It is known that, if the laser frequency is tuned around resonances, field-dressed states originating from different Floquet blocks (and corresponding to the coupled field-free states) display avoided crossings. These crossings have been shown to be related to localization, and to chaos in the corresponding classical system [19]. The separation of the two dressed states involved corresponds to the Rabi frequency and is proportional to the field strength of the driving laser. We will now show that the same is observed for transitions between

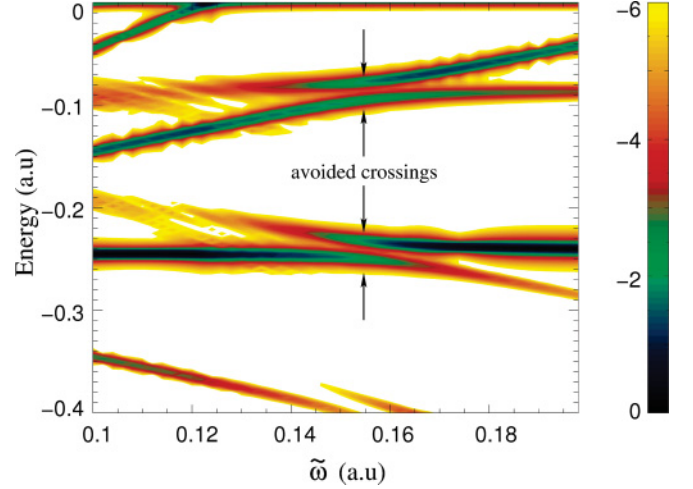


FIG. 4. (Color online) R vs energy \mathcal{E} and second-laser frequency $\tilde{\omega}$ for first-laser excursion $\hat{\alpha} = 2.5$ and second-laser field strength amplitude $\tilde{E} = 0.01$.

already-dressed states; that is, we use a laser of frequency ω_1 to dress the system and a second, weaker laser, of frequency $\tilde{\omega}$ to induce transitions between dressed states. The second laser will dress the already-dressed system [20], and the “dressed²” states (or two-color-dressed states) should display avoided crossings as the frequency $\tilde{\omega}$ is tuned around the energy gap of two dressed states.

From Fig. 2 one infers that, for an excursion amplitude $\hat{\alpha} = 2.5$, the energy difference between the field-dressed ground state and the field-dressed first excited state is $\text{Re}\epsilon_1 - \text{Re}\epsilon_0 \simeq 0.155$. Hence, we tune the frequency $\tilde{\omega}$ of the second laser around this energy difference. The pulse envelope was the same for both lasers, and the electric field amplitude of the second laser was $\tilde{E} = 0.01 = \tilde{A}\tilde{\omega} = \hat{\alpha}\tilde{\omega}^2$ for all $\tilde{\omega}$. Figure 4 shows results for the Floquet energy spectrum R vs energy and $\tilde{\omega}$ for $\hat{\alpha} = 2.5$. If the two frequencies ω_1 and $\tilde{\omega}$ are incommensurate, the Hamiltonian is not periodic at all. However, our approach does not require periodicity, and we expect a Floquet analysis to be meaningful as long as the two-color Hamiltonian is *approximately* periodic; namely, in $\tilde{T} = 2\pi/\tilde{\omega}$ because $\omega_1 \gg \tilde{\omega}$. In fact, the avoided crossings of $\text{Re}\epsilon_0$ with $\text{Re}\epsilon_1 - \tilde{\omega}$ and of $\text{Re}\epsilon_0 + \tilde{\omega}$ with $\text{Re}\epsilon_1$ around $\tilde{\omega} = 0.155$ are clearly visible in Fig. 4.

V. TRANSFORMATIONS

We consider transformations $\hat{G}(t)$ which are periodic in time and reduce to unity as the laser field goes to zero,

$$\hat{G}(t + T) = \hat{G}(t), \quad \hat{G}(t)|_{\alpha, E, A=0} = \hat{1}. \quad (39)$$

Now, since each Floquet state Φ_{β} fulfills (8),

$$\hat{G}(t)\hat{\mathcal{H}}(t)\hat{G}^{-1}(t)\hat{G}(t)|\Phi_{\beta}(t)\rangle = \hat{\mathcal{H}}'(t)|\Phi'_{\beta}(t)\rangle = \epsilon_{\beta}|\Phi'_{\beta}(t)\rangle, \quad (40)$$

where $\hat{\mathcal{H}}'(t) = \hat{G}(t)\hat{\mathcal{H}}(t)\hat{G}^{-1}(t)$ is the transformed Floquet-Hamiltonian and $|\Phi'_{\beta}(t)\rangle = \hat{G}(t)|\Phi_{\beta}(t)\rangle$ is the transformed Floquet state. The quasienergy ϵ_{β} is not affected by the

transformation, and $|\Phi'_\beta(t)\rangle$ is also periodic because of (39), so that with (11)

$$\sum_n e^{-in\omega_1 t} |\varphi'_{\beta n}\rangle = \sum_{nm} e^{-i(n+m)\omega_1 t} \hat{G}_m |\varphi_{\beta n}\rangle, \quad (41)$$

where $\hat{G}(t) = \sum_m e^{-im\omega_1 t} \hat{G}_m$, and thus

$$|\varphi'_{\beta \ell}\rangle = \sum_n \hat{G}_{\ell-n} |\varphi_{\beta n}\rangle. \quad (42)$$

We now specialize on transformations \hat{G} that commute with the dynamical symmetry operation \hat{P}_{pt} ,

$$[\hat{G}(t), \hat{P}_{pt}] = 0. \quad (43)$$

Examples are gauge transformations, for example, for the transformation from the velocity gauge, where

$$\hat{W}(t) = \hat{p}A(t) + \frac{1}{2}A^2(t), \quad (44)$$

to the length gauge, one has

$$G_{LG}(t) = \exp[ixA(t)]. \quad (45)$$

Another example is the Pauli-Fierz or Kramers-Henneberger (KH) transformation, which is *not* a gauge transformation (although one frequently finds the term ‘‘KH gauge’’ in the literature). If we start from the velocity gauge interaction (44) the KH transformation reads

$$\hat{G}_{KH}(t) = \exp\left[\frac{i}{2} \int_{-\infty}^t A^2(t') dt' + i\alpha(t)\hat{p}\right]. \quad (46)$$

This amounts to a translation in position space by the free electron excursion $\alpha(t)$ (31) and a purely time-dependent contact transformation. The KH Floquet-Hamiltonian is

$$\hat{\mathcal{H}}'(t) = \hat{\mathcal{H}}_{KH}(t) = \frac{1}{2}\hat{p}^2 + V[x + \alpha(t)] - i\frac{\partial}{\partial t}. \quad (47)$$

As a consequence of (43),

$$\hat{P}_{pt}|\Phi'_\beta(t)\rangle = \hat{G}(t)\hat{P}_{pt}|\Phi_\beta(t)\rangle = \pm|\Phi'_\beta(t)\rangle, \quad (48)$$

with the eigenvalue ± 1 the same as for $\hat{P}_{pt}|\Phi_\beta(t)\rangle = \pm|\Phi_\beta(t)\rangle$. One also finds $\hat{G}_m = (-1)^m \hat{P}_p \hat{G}_m \hat{P}_p$ and $\hat{P}_p |\varphi'_{\beta \ell}\rangle = \pm(-1)^\ell |\varphi_{\beta \ell}\rangle$; that is, the transformed (primed) states have the same symmetry as the original states.

Figure 5 shows the KH and the velocity gauge probability density for the excursion amplitude $\hat{\alpha} = 10$. The target energy was $\mathcal{E} = -0.08$ where, in Fig. 2, the almost-degenerate ground- and first-excited-state energies for $\hat{\alpha} = 10$ are located. The KH probability density fits to the KH potential

$$V_{KH}(x) = \frac{1}{2\pi} \int_0^{2\pi} V[x + \hat{\alpha} \sin \tau] d\tau, \quad (49)$$

shown in the lower panel. The actual calculation was performed for $\omega_1 = 4$ and a trapezoidal (10, 1180, 10) pulse. The target energy \mathcal{E} in (37) is scanned through the energy region of interest, and the Floquet energy is hit when the value of the integral is maximum. If one uses the same integration time for different \mathcal{E} , the integral

$$N_{\mathcal{E}} = \int_{-\frac{l}{2}}^{\frac{l}{2}} |\varphi_{\mathcal{E}}(x)|^2 dx \quad (50)$$

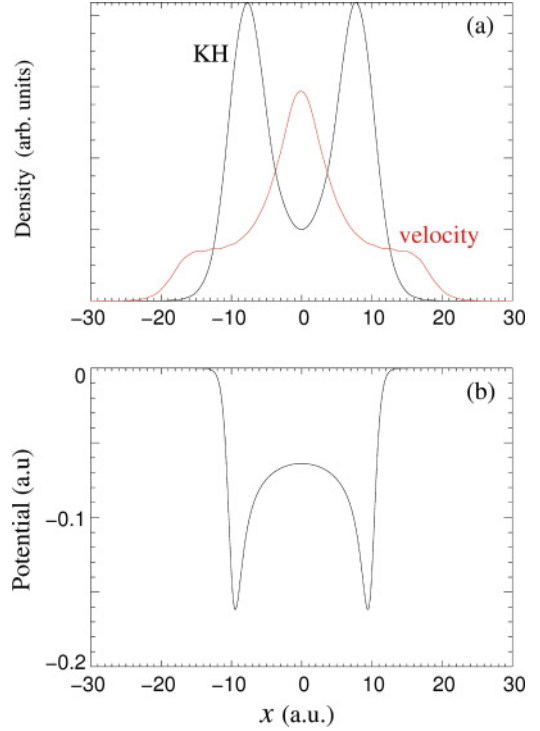


FIG. 5. (Color online) (a) KH and the velocity-gauge probability density for the excursion amplitude $\hat{\alpha} = 10$ and target energy $\mathcal{E} = -0.08$. (b) Corresponding KH potential.

is a relative measure for the population of the respective Floquet state in the actual pulse.

The Floquet energies are invariant under the transformations $\hat{G}(t)$ while both the Floquet states $|\varphi_{\beta n}\rangle$ and their populations are not. In particular, in the high-frequency limit one expects that only the eigenstates in the KH potential (49) matter [9]. These states correspond to the Floquet energies in the Floquet block $n = 0$. Hence, the energy spectrum in the KH frame is expected to be much more localized around $n = 0$ than in velocity gauge. This is confirmed by Fig. 6. Instead of using the even or odd test functions in (35) and spatial integration we analyzed the wave function $\Psi_{\#}(x, t)$ at $x_{\text{test}} = 2$; that is, we calculated

$$Q'(\mathcal{E}) = \sum_{\beta n} \int_{t_1}^{t_2} e^{-it(\epsilon_{\beta} + n\omega_1 - \mathcal{E})} dt \varphi_{\beta n}(x_{\text{test}}). \quad (51)$$

This avoids the transformation of the entire wave function to the KH frame and yields similar results as long as one chooses x_{test} in a region where the wave function is sizable and both odd and even parity wave functions contribute (for $x_{\text{test}} = 0$ only contributions from even Floquet states would be visible). Figure 6 confirms that, for transformations of the type (39), the populations of Floquet states in different frames (or gauges) are different while the Floquet energies are the same. The latter, dressed levels could be probed with a second laser [21]. Of course, any gauge or frame dependence should vanish when field-free observables, such as photoelectron spectra, are considered.

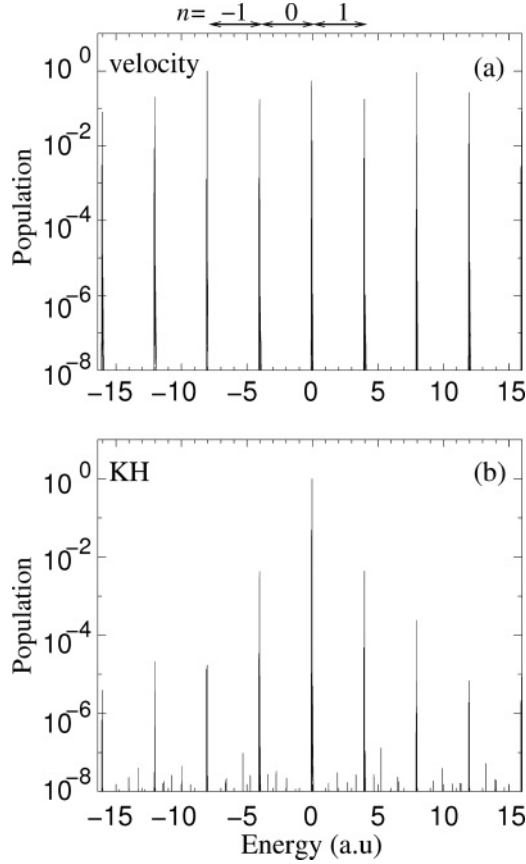


FIG. 6. Floquet spectra for $\hat{\alpha} = 10$, $\omega_1 = 4$, and a (10, 1180, 10) pulse in (a) velocity gauge [with the $A^2(t)/2$ term transformed away] and (b) in the KH frame. In the KH frame the $n = 0$ Floquet block dominates while in velocity gauge the population is broadly distributed over many Floquet blocks.

VI. PHOTOELECTRON SPECTRA

Without the laser field the continuum states of the Pöschl-Teller potential have energies $\mathcal{E} > 0$. With the laser field all continuum and bound states are contained in each Floquet block so that overlaps of dressed bound states from one block with continua from other blocks with lower n are possible. However, we expect the dressed bound states of the $n = 0$ block to dominate since they are the main ones being populated during the switching on of the laser. Let us first discuss the case where $\omega_1 > \min \text{Re}\epsilon_\beta$, i.e., a single photon is sufficient for ionization. Then the dressed bound state in Floquet block n with energy $\text{Re}\epsilon_\beta + n\omega_1$ overlaps with continuum states of all the Floquet blocks $m < n$. In particular, $\text{Re}\epsilon_\beta + n\omega_1$ overlaps with the continuum state of energy ϵ_p of the zeroth Floquet block, where p indicates the asymptotic momentum of this continuum state.

We will now turn to the question of how the manifold of mixtures of bound and continuum Floquet states converts to an observable photoelectron spectrum when the pulse is switched off. Figure 7 shows a time-resolved Floquet spectrum in velocity gauge for a $N_{\text{cyc}} = 100$ -cycle- \sin^2 pulse

$$A(t) = \hat{A} \sin^2\left(\frac{\omega_1 t}{2N_{\text{cyc}}}\right) \sin \omega_1 t, \quad (52)$$

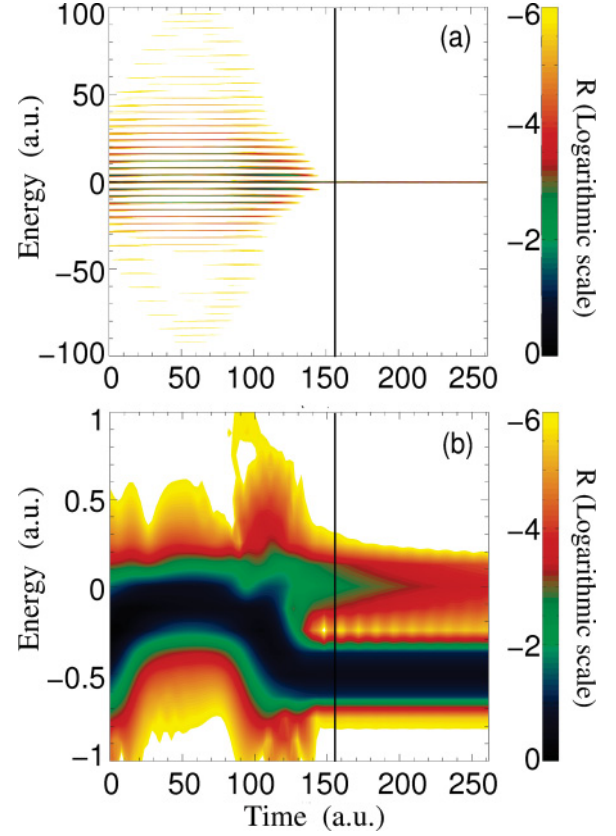


FIG. 7. (Color online) Time-resolved Floquet spectra for a 100-cycle- \sin^2 pulse of amplitude $\hat{\alpha} = \hat{A}/\omega_1 = 10$, $\omega_1 = 4$, $x_{\text{test}} = 2$ (i.e., “inside” the potential), and a time window of width $t_w = t_2 - t_1 = 50$. The vertical line indicates the end of the pulse. Panel (b) is a close up of the energy region around $\epsilon_0^{(0)} = -0.5$ in (a). The calculation was performed in the velocity gauge [with the $A^2(t)/2$ term transformed away].

for $0 < t < N_{\text{cyc}}2\pi/\omega_1$ and zero otherwise. The other pulse parameters are given in the figure caption, and $x_{\text{test}} = 2$ (i.e., “inside” the potential) and a time window of width $t_w = t_2 - t_1 = 50$ were chosen for (51). The time on the horizontal axis is t_1 so that the spectrum for times $t_1 > 100T = 157.1$ (indicated by the vertical black line) shows field-free states; that is,

$$\begin{aligned} Q^{(0)}(\mathcal{E}, t_1) &= \int_{t_1}^{t_1+t_w} e^{i\mathcal{E}t} \Psi_{\#}(x_{\text{test}}, t) dt \\ &= \sum_{\beta} \varphi_{\beta}^{(0)}(x_{\text{test}}) \int_{t_1}^{t_1+t_w} e^{-it(\epsilon_{\beta}^{(0)} - \mathcal{E})} dt. \end{aligned} \quad (53)$$

Figure 7(a) shows that, while the pulse is on, the population is distributed over many Floquet blocks. As the pulse is switched off, all the Floquet populations for $n \neq 0$ disappear, and only the ground-state population inside the potential with energy $\epsilon_0^{(0)}$ remains. This is because we analyzed the spectrum at the position $x_{\text{test}} = 2$. Contributions to the wave function corresponding to electrons in the continuum, traveling with an asymptotic momentum p , decay at $x_{\text{test}} = 2$. Figure 7(b) shows a close-up of the region around $\epsilon_0^{(0)}$. With increasing amplitude of the laser pulse the dominant Floquet population shifts adiabatically from the field-free value $\epsilon_0^{(0)} = -0.5$ to the

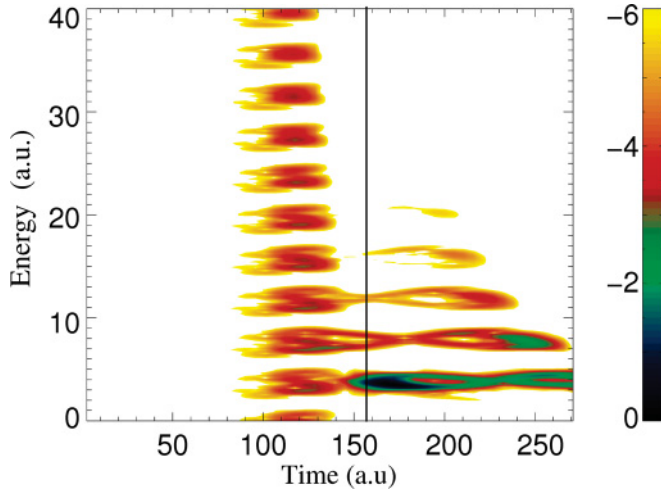
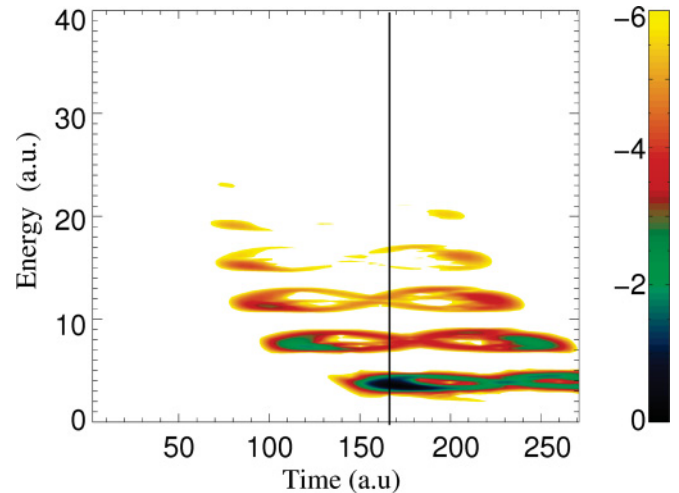
FIG. 8. (Color online) Same as in Fig. 7 but for $x_{\text{test}} = 471.3$.

FIG. 9. (Color online) Same as Fig. 8 but in the KH frame.

ground-state energy of the KH potential $\epsilon_0^{(\text{KH})} \simeq -0.09$ (see Fig. 2 for $\hat{\alpha} = 10$) and back. Note that, although the calculation was performed in velocity gauge, the KH ground-state energy is relevant here because the Floquet quasienergies are frame and gauge independent.

Figure 8 shows the same analysis for $x_{\text{test}} = 471.3$ (i.e., “far away” from the atom) so that it takes some time until probability density arrives there; namely, around $t = 100$. It is interesting to observe that, in the velocity gauge, this “arrival time” during the pulse is independent of the energy. As the laser pulse is switched off at $t = 157.1$ many Floquet channels close. However, because electrons are still on their way from the atom to the “virtual detector” at $x_{\text{test}} = 471.3$ we are able to “measure” the field-free photoelectron spectrum of the electrons emitted in that direction. The time that these free electrons need to pass the virtual detector decreases with increasing energy, as is seen in Fig. 8 where the width of the traces for $t > 157.1$ decreases with increasing energy. The five traces visible are separated by ω_1 and correspond to above-threshold-ionization (ATI) peaks (see, e.g., the review [22] or [23]). They are quite broad in energy because of the change of the ionization potential (from the field-free value to the KH value and back). Their figure-eight shape in the contour plot of Fig. 8 is a peculiarity of the \sin^2 pulse shape.

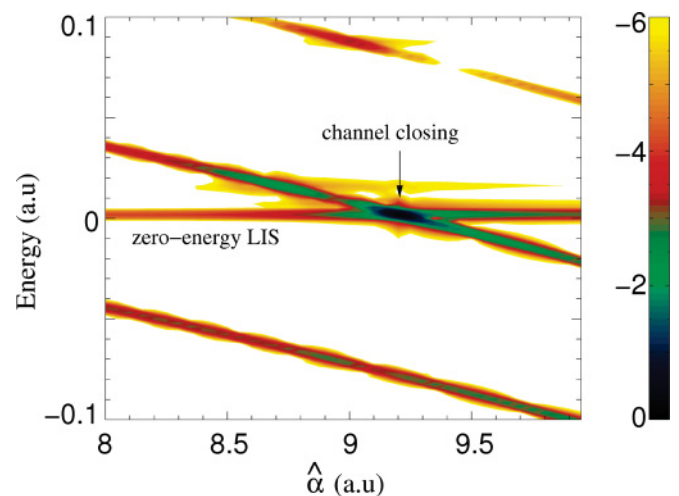
Figure 9 shows the corresponding result obtained in the KH frame. We see that, in the KH frame, only those states are populated in the laser field which actually contribute to the final field-free spectrum. This is because the KH potential at $x_{\text{test}} = 471.3$ is almost identical to the field-free potential so that outgoing electrons are not affected anymore by the oscillating KH binding potential. It is also seen in Fig. 9 that the most energetic electrons arrive earlier at x_{test} , unlike the velocity-gauge result in Fig. 8.

VII. CHANNEL CLOSINGS

So far, we studied mainly high-frequency phenomena where the Floquet blocks are well separated on the atomic energy scale because the laser frequency exceeds the ground-state

ionization potential. However, there are plenty of interesting, nonperturbative phenomena occurring at low frequencies where the ponderomotive energy $U_p = \hat{E}^2/(4\omega_1^2)$ can be large at currently available laser intensities \hat{E}^2 . Examples are tunneling ionization and high-order ATI due to rescattering of electrons [23,24]. In this section we choose the so-called “channel closing” (see [25] and references therein) as a low-frequency phenomenon to illustrate our method.

The TDSE was solved for a trapezoidal pulse of frequency $\omega_1 = 0.08$. On the energy scale of the ionization potential the Floquet blocks are packed much closer in this case, meaning that many photons are necessary for ionization. In Fig. 10 we plot the Floquet energy spectrum R in a certain range of excursion amplitude $\hat{\alpha} = \hat{E}/\omega_1^2$ and energy \mathcal{E} around the field-free continuum threshold (other relevant parameters given in the figure caption). The calculation was performed in the velocity gauge using again the potential (30). There is a clear downshift of all the populated Floquet levels with increasing laser amplitude. This ac Stark shift is also

FIG. 10. (Color online) Logarithmic plot of $R = |Q_+|^2 + |Q_-|^2$ vs energy \mathcal{E} and excursion amplitude $\hat{\alpha}$, showing the (populated) field-dressed states for $\omega_1 = 0.08$ and a trapezoidal (4, 40, 4) pulse.

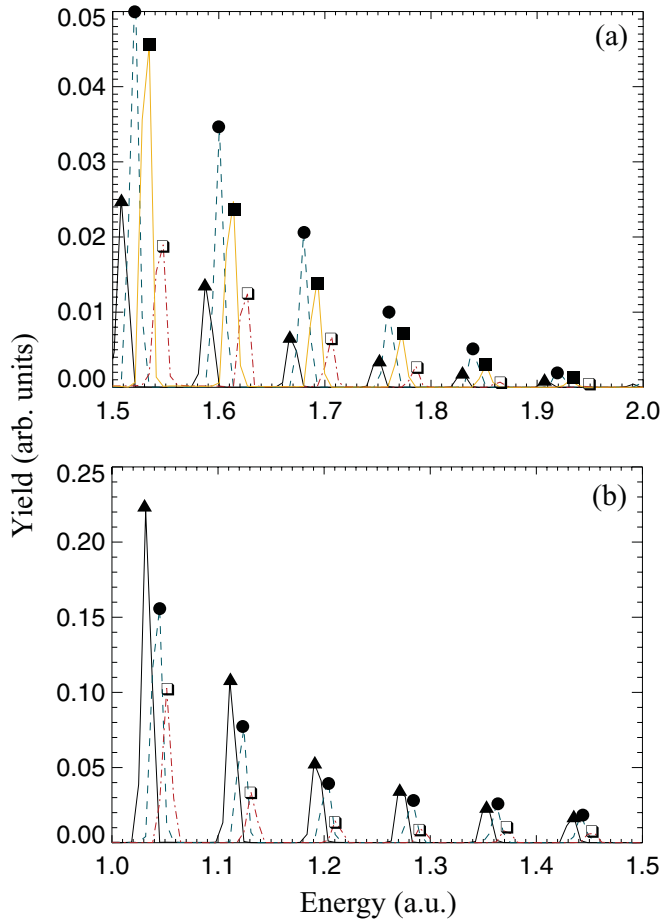


FIG. 11. (Color online) Photoelectron spectra around $5U_p$ with the same parameters as in Fig. 10. (a) Nonmonotonic behavior of the yield (open squares $\hat{\alpha} = 13.0$, solid squares 13.3, circles 13.55, triangles 13.8). (b) Same for an odd channel closing, showing a monotonic behavior of the yield with increasing intensity (triangles $\alpha = 11.8$, circles 11.55, open squares $\alpha = 11.3$).

referred to as the “ponderomotive shift” because the effective ionization potential is increased by U_p . In fact, the energy in the photoelectron spectrum is given by

$$\mathcal{E} = \frac{p^2}{2} = n\hbar\omega_1 - (|\mathcal{E}_0| + U_p) \quad (54)$$

(provided the ac Stark shift of the initial state is negligible, which for atomic ground states at long wavelengths is often the case). \mathcal{E}_0 is the initial electron energy and n is the number of photons absorbed. In order to reach the continuum at all $n > (|\mathcal{E}_0| + U_p)/(\hbar\omega_1)$ photons have to be absorbed. As the intensity, and thus U_p , is increased, more and more photons are needed for ionization. When n photons are no longer sufficient but $n + 1$ photons are needed, the n -photon channel closing occurs. In the plot shown in Fig. 10 a channel closing manifests itself as a crossing of a Floquet quasienergy and the continuum threshold. Now, the interesting feature in Fig. 10 is the zero-energy LIS. Such LISs were also observed in Ref. [26], where their connection with experimentally observed enhancements in the photoelectron spectra at high energies [27] was established. The parity of both states involved in the crossing in

Fig. 10 is even, and it is known that, depending on the parity of the states, channel closings affect the photoelectron spectrum differently [26,28].

In our model, for the first even channel closing, eight photons are needed. According to (54), it is expected at $\hat{\alpha} = 9.354$, which indeed is close to where the crossing is observed in Fig. 10. The small discrepancy is because of the ac Stark shift of the initial state, neglected in (54). One would expect that channel closings only affect low-energy electrons because the kinetic energy of the electrons whose channel is about to close is low. Hence, as the intensity is increased the yield of ATI peaks at energies, say, $>5U_p$ should increase monotonically as well. However, near even-photon channel closings there is a marked increase in the photoelectron yield at high energies [25,26,28]. Instead, when in odd-photon channel closings the odd-parity LIS crosses the zero-energy LIS, and such enhancements are absent. The first odd-photon channel closing occurs around $\hat{\alpha} = 11.55$, the next even-photon channel closing occurs around $\hat{\alpha} = 13.55$. The photoelectron spectra obtained using our Floquet method confirm the presence and absence of enhancements at even and odd channel closings, respectively, as shown in Fig. 11.

VIII. CONCLUSIONS

We described a method for obtaining Floquet information from real-time wave functions. In this approach, it is not necessary to assume strict periodicity. In fact, it is possible to follow the time-resolved Floquet quasienergies as they shift during a laser pulse. Moreover, the populations of the Floquet states can be determined so that, especially, cases where superpositions of Floquet states play a role can be identified. The usefulness of the method was illustrated by several examples employing the one-dimensional Pöschl-Teller potential with only a single field-free bound state. In particular, we discussed the origin of peaks at even harmonics of the laser frequency in an inversion-symmetric potential, avoided crossings of dressed already field-dressed states induced by a second laser, the properties of Floquet states under time-periodic transformations, the emergence of invariant, observable photoelectron spectra after the laser pulse, and photoelectron enhancements at channel closings. The method is straightforwardly extendable to three dimensions. We think the method is most useful for researchers running codes to solve the time-dependent Schrödinger equation in real time. By saving the wave function at selected spatial positions as a function of time during the interaction with the laser field, the analysis in terms of light-induced states can be easily performed *a posteriori*. The application of the method to correlated multielectron systems may be very fruitful, because the understanding of field-dressed, multiply excited or autoionizing states is still poor.

ACKNOWLEDGMENTS

This work was supported by the SFB 652 of the German Science Foundation (DFG).

APPENDIX: EXTENSION TO THREE DIMENSIONS

The method of Floquet analysis described in this work is easily extendable to higher-dimensional systems. For example, for hydrogenic systems in three dimensions (3D), one could follow the evolution of Floquet states with different orbital angular momentum quantum numbers l . Instead of (6) we have

$$\Psi(r, \theta, \phi, t) = e^{-i\epsilon t} \Phi(r, \theta, \phi, t), \quad (\text{A1})$$

with [compare to (11)]

$$\Phi(r, \theta, \phi, t) = \sum_n \varphi_n(r, \theta, \phi) e^{-in\omega_1 t}. \quad (\text{A2})$$

The operator \hat{P}_{pt} [compare to (21)] acts according to

$$\hat{P}_{pt} f(\mathbf{r}, t) = f\left(-\mathbf{r}, t + \frac{\pi}{\omega_1}\right), \quad (\text{A3})$$

and (24) becomes

$$\begin{aligned} \hat{P}_{pt} \Phi(r, \theta, \phi, t) \\ = \sum_n (-1)^n \exp(-in\omega_1 t) \hat{P}_p \varphi_n(r, \theta, \phi). \end{aligned} \quad (\text{A4})$$

If we expand the $\varphi_n(r, \theta, \phi)$ in spherical harmonics,

$$\varphi_n(r, \theta, \phi) = R_{nl}(r) Y_{lm}(\theta, \phi), \quad (\text{A5})$$

we find, using

$$\hat{P}_p Y_{lm}(\theta, \phi) = Y_{lm}(\pi - \theta, \pi + \phi) = (-1)^l Y_{lm}(\theta, \phi), \quad (\text{A6})$$

that

$$\hat{P}_p \varphi_n(r, \theta, \phi) = (-1)^{n+l} \varphi_n(r, \theta, \phi), \quad (\text{A7})$$

the analog of (25). Note that n is the Floquet block index here, not the principal quantum number. After these considerations it is straightforward to extend the Floquet analysis of real-time wave functions described in this work to 3D.

-
- [1] M. G. Floquet, *Ann. Écol. Norm. Sup.* **12**, 47 (1883).
 [2] J. H. Shirley, *Phys. Rev.* **138**, B979 (1965); H. Sambe, *Phys. Rev. A* **7**, 2203 (1973).
 [3] Floquet theory is covered in several text books, such as D. J. Tannor, *Introduction to Quantum Mechanics: a Time-Dependent Perspective* (University Science Books, Sausalito, 2007); B. H. Bransden, and C. J. Joachain, *Physics of Atoms and Molecules* (Prentice Hall, Harlow, 2003); H. Friedrich, *Theoretical Atomic Physics*, (Springer, Berlin, 2006); F. H. M. Faisal, *Theory of Multiphoton Processes* (Plenum Press, New York, 1987).
 [4] S.-I. Chu and D. A. Telnov, *Phys. Rep.* **390**, 1 (2004).
 [5] R. M. Potvliege, *Phys. Scr.* **68**, 18 (2003).
 [6] R. M. Potvliege and R. Shakeshaft, *Phys. Rev. A* **38**, 4597 (1988); **40**, 3061 (1989).
 [7] R. M. Potvliege, *Comput. Phys. Commun.* **114**, 42 (1998).
 [8] P. G. Burke, P. Francken, and C. J. Joachain, *J. Phys. B* **24**, 761 (1991); H. W. van der Hart, M. A. Lysaght, and P. G. Burke, *Phys. Rev. A* **76**, 043405 (2007).
 [9] M. Gavrilin, *J. Phys. B* **35**, R147 (2002).
 [10] R. Grobe and M. V. Fedorov, *Phys. Rev. Lett.* **68**, 2592 (1992); **69**, 3591(E) (1992).
 [11] A. E. Kazakov, V. P. Makarov, and M. V. Fedorov, *Sov. Phys. JETP* **43**, 20 (1976) [*Zh. Eksp. Teor. Fiz.* **70**, 38 (1976)].
 [12] M. V. Fedorov and A. E. Kazakov, *Prog. Quantum Electron.* **13**, 1 (1989).
 [13] O. E. Alon, V. Averbukh, and N. Moiseyev, *Phys. Rev. Lett.* **80**, 3743 (1998); O. E. Alon, *Phys. Rev. A* **66**, 013414 (2002).
 [14] F. Ceccherini, D. Bauer, and F. Cornolti, *J. Phys. B* **34**, 5017 (2001).
 [15] R. Bavli and H. Metiu, *Phys. Rev. A* **47**, 3299 (1993).
 [16] N. Moiseyev and M. Lein, *J. Phys. Chem. A* **107**, 7181 (2003).
 [17] A. Di Piazza and E. Fiordilino, *Phys. Rev. A* **64**, 013802 (2001).
 [18] M. D. Feit, J. A. Fleck, and A. Steiger, *J. Comput. Phys.* **47**, 412 (1982).
 [19] T. Timberlake and L. E. Reichl, *Phys. Rev. A* **59**, 2886 (1999).
 [20] S. S. Shamailov, A. S. Parkins, M. J. Collett, and H. J. Carmichael, *Opt. Commun.* **283**, 766 (2010).
 [21] F. Morales, M. Richter, S. Patchkovskii, and O. Smirnova, *PNAS* **108**, 16906 (2011).
 [22] W. Becker, F. Grasbon, R. Kopold, D. B. Milošević, G. G. Paulus, and H. Walther, *Adv. At. Mol. Opt. Phys.* **48**, 35 (2002).
 [23] See, e.g., P. Mulser and D. Bauer, *High Power Laser-Matter Interaction* (Springer, Berlin Heidelberg, 2010), Chap. 7.
 [24] D. B. Milošević, G. G. Paulus, D. Bauer, and W. Becker, *J. Phys. B* **39**, R203 (2006).
 [25] B. Fetić, D. B. Milošević, and W. Becker, *J. Mod. Opt.* **58**, 1149 (2011).
 [26] J. Wassaf, V. Vénier, R. Taïeb, and A. Maquet, *Phys. Rev. Lett.* **90**, 013003 (2003); *Phys. Rev. A* **67**, 053405 (2003).
 [27] M. P. Hertlein, P. H. Bucksbaum, and H. G. Muller, *J. Phys. B* **30**, L197 (1997); P. Hansch, M. A. Walker, and L. D. Van Woerkom, *Phys. Rev. A* **55**, R2535 (1997); G. G. Paulus, F. Grasbon, H. Walther, R. Kopold, and W. Becker, *ibid.* **64**, 021401(R) (2001).
 [28] S. V. Popruzhenko, Ph. A. Korneev, S. P. Goreslavski, and W. Becker, *Phys. Rev. Lett.* **89**, 023001 (2002).